IEEE Access
Multidisciplinary | Rapid Review | Open Access Journal

Received 7 June 2023, accepted 23 June 2023, date of publication 28 June 2023, date of current version 6 July 2023.

Digital Object Identifier 10.1109/ACCESS.2023.3290898

RESEARCH ARTICLE

A New Technique for Radial and Tangential Force Calculation Time Reduction for the Optimization Process of SRMs

MOHAMED ABDALMAGID[1,2], (Graduate Student Member, IEEE), MOHAMED H. BAKR[1], (Senior Member, IEEE), AND ALI EMADI[1], (Fellow, IEEE)

[1]Department of Electric and Computer Engineering, McMaster University, Hamilton, ON L8S 4S4, Canada
[2]Department of Power Electronics and Energy Conversion Systems, Electronics Research Institute, Cairo 12622, Egypt

Corresponding author: Mohamed Abdalmagid (abdelm47@mcmaster.ca)

ABSTRACT This article introduces a new technique for reducing the time of calculating radial and tangential force density waves of switched reluctance machines (SRMs). The method is based on the finite element (FE) simulation of a fraction of an electrical cycle. The new approach shows that a significant time reduction is achieved as compared to the time required for stator radial force density and the rotor tangential force calculation based on the one mechanical cycle simulation method. As the switched reluctance motors introduce new challenges in aspects such as acoustic noise, vibrations, and torque ripples, the method introduced in this paper will help reduce the time of the optimization process of switched reluctance machines in the design stage to improve the machine performance. The proposed method is applied to radial flux SRMs. Three different topologies were used to show the effectiveness of this technique in different force components with minimal error as compared to the benchmark method based on the FE simulation of one mechanical cycle.

INDEX TERMS Radial force, switched reluctance machine, tangential force, torque ripples.

I. INTRODUCTION

Nowadays the performance improvement of Switch Reluctance Motors (SRMs) is attractive. Due to the continuously increasing price of rare-earth permanent magnets (PMs), extensive research focuses on removing or reducing the PMs from the design of electrical machines. Also, the absence of the windings and magnets from the rotor enables the SRM to run at high speed and elevated temperatures [1]. Typically, concentrated winding is employed for the stator of Switched Reluctance Motors (SRMs), which have the advantage of lower costs for machine assembly and upkeep. The concentrated winding approach improves the fault-tolerance ability of the SRMs as it decreases the magnetic coupling between the machine's phases [2]. In addition to a simple and sturdy design, Switched Reluctance Motors (SRMs) offer significant advantages such as affordability [1]. The aforementioned advantages in SRMs make them a perfect option for various applications [3], [4], [5]. Despite the benefits of SRMs, the double salient structure of the machine presents certain difficulties, such as excessive acoustic noise, vibrations, and notable torque ripples in the machine [1].

In the radial flux SRM configurations, the mean torque is produced by the DC component of the tangential force density acting on the rotor. The DC component of the tangential force density is the component that has zero temporal order and zero circumferential order. That component of the tangential force density wave of a three-phase 6/4 SRM is indicated by the central red cell in Figure 1. However, The torque ripples of the machine are generated due to all the other rotor tangential force density components with zero circumferential order. These rotor tangential force density components are shown in Figure 1 with orange colour along the temporal order axis. The paper proves that the DC component is responsible for the mean torque, and all the other rotor tangential force components with zero circumferential

The associate editor coordinating the review of this manuscript and approving it for publication was Xuebo Zhang.

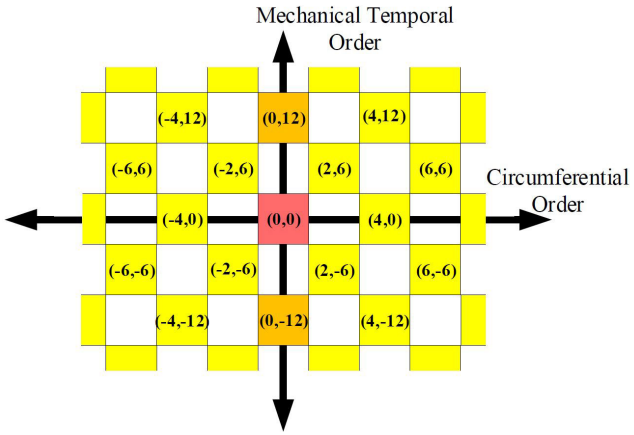

FIGURE 1. A graphical representation of a part of the rotor tangential force density components for a 6/4 SRM.

order are responsible for the torque ripples of the machine. The other rotor tangential force density components with temporal orders other than zero (shown in Figure 1 by the yellow cells) cause the rotor structure's acoustic noise and vibration [6].

To improve the machine's performance, the DC component of the rotor tangential force density should be maximized, and all the other rotor tangential force density components should be minimized. The most significant force density components that significantly affect the torque ripples and acoustic noise should be selected for the optimization process. The most significant force density components are the components that can excite the machine's different vibration modes and result in elevated levels of acoustic noise and vibration [7]. The stator tangential force components of high amplitude can also excite the natural frequencies of the main tangential stator modes for the external rotor machine [8].

In the inner rotor SRM configurations, the radial force acting on the stator is the primary source of the machine's acoustic noise and vibrations [9]. In that case, the machine structure can be optimized to reduce the radial force density components that have the most impact in exciting the natural frequencies of main radial stator modes [10], [11]. The radial force acting on the rotor structure in the external rotor SRMs configurations also contributes to that configuration's acoustic noise and vibrations [8]. In order to reduce the acoustic level and vibrations of external rotor SRM configurations, the radial force density components of the rotor and the tangential force density components of the stator should be minimized [8].

One of the ways to reduce the SRMs' acoustic noise and vibrations is through structural optimization by shifting the frequency of the critical circumferential vibration modes to avoid exciting these vibration modes with the force density components [13]. Another way is to reduce the amplitude of the critical force density components that can excite the vibration modes of the machine structure through electromagnetic optimization of the key design parameters of the machine [14], [15]. Optimizing the control parameters was used in the literature also to reduce the amplitude of the critical force density components of the machine for the same purpose [16], [17]. The reader can refer to [1], [10], and [18] for more information about the interaction between the force components and the SRMs circumferential vibration modes.

The optimization process to decrease the acoustic noise and vibration of SRMs requires evaluating the radial force and tangential force density components at each iteration of the optimization process. The evaluation process is usually based on Finite element analysis (FEA) simulation of one mechanical cycle to obtain stator and rotor force density wave components [12]. The study in [10] shows that the stator force density wave components can be estimated based on the FEA simulation of one electrical cycle. However, this method cannot be applied to the rotor force density components as the FEA simulation of one mechanical cycle is required to get the accurate rotor force density components. This point is illustrated throughout this paper.

The geometrical parameters optimization of SRMs for acoustic noise reduction required multiple evaluations of the objective function as discussed in [1], [13], [19], and [20]. The drive control parameters are also used in the literature for the acoustic noise reduction of the SRMs [21], [22], [23], [24] which also needs multiple calculations of the radial force and tangential force components of the machine. The multi-objective optimization of SRMs, such as presented in [25], makes the optimization process very time-consuming. In [26], machine learning techniques used for the torque ripple minimization and the acoustic noise mitigation are illustrated. The optimization techniques based on machine learning require a high number of objective function evaluations, and any reduction in the objective function calculation time will result in a huge reduction in the optimization time. It is clear that the computational cost of calculating the radial force, tangential force, and torque wave components is a common problem between these methods. In this paper, we are proposing a new technique to reduce the computational time of calculating the radial force, the tangential force components, and the torque wave components to solve this problem. The new technique is expected to reduce the optimization time significantly by reducing the force calculation time, as presented in this paper.

This work introduces a new technique for generating the stator radial force density wave and the rotor tangential force density wave based on the FEA simulation of $1/N_{ph}$ of an electrical cycle, where N_{ph} is the number of the machine phases. The method can help reduce the force calculation time and hence the optimization time compared to the classical ways of calculating the force density waves of SRMs.The new method is applied to three different SRM configurations (three-phase 6/4 SRM, three-phase 6/14 SRM, and four-phase 8/6 SRM). The method shows a considerable time reduction and low computational effort as compared to the one mechanical cycle technique of obtaining the SRM force density waves.

The rest of the paper is divided as follows. Section II presents the methods used in the literature to generate the stator force density waves using one mechanical cycle simulation and one electrical cycle simulation. Section II also presents the new fractional of an electrical cycle technique in generating one repetition of the SRMs stator force density wave. Section III shows the conventional method used for obtaining the rotor tangential force density wave based on the finite element simulation of a complete mechanical cycle. Section III also presents the new fractional of an electrical cycle method for generating one repetition of SRMs rotor tangential force density wave. Sections IV and V show numerical examples of applying the fraction of the electrical cycle method to three different case studies for generating the stator radial force density components and the rotor tangential force density components and the comparison with the existing methods.

II. STATOR FORCE DENSITY DECOMPOSITION METHODS

This section reviews the methods of stator force decomposition illustrated in the literature. A newly proposed method based on the simulation of a fraction of an electrical cycle is also presented. The new approach reduces the number of FEA simulation steps needed to calculate the stator force density wave and hence the time required to calculate the stator force density components required for the optimization purpose at the design stage of the machine.

A. STATOR RADIAL FORCE DENSITY COMPONENTS CALCULATION BASED ON ONE MECHANICAL CYCLE AND ONE ELECTRICAL CYCLE

The radial force density is usually calculated on the stator structure of the SRMs to evaluate and reduce the machine's acoustic noise and vibration. The radial force density pattern is given by [6]:

$$\begin{cases} u = N_r \times N_{ph} \times j - N_r \times k \\ v = \frac{N_s}{N_{ph}} k \end{cases} \quad (1)$$

where u is the harmonic's the mechanical temporal order, v is the harmonic's circumferential order, N_s is the number of stator teeth, N_r is the number of rotor teeth, N_{ph} is the number of the machine phases, and j and k are integer numbers [6]. As indicated in [6], the stator radial force density and the stator tangential force density components have the same pattern, which is given by (1). The discussion in this article will be limited to the stator radial force density decomposition. However, the same analysis can be used for the stator tangential force density decomposition.

Based on (1), the greatest common division (GCD) of all the mechanical temporal orders of the radial force density acting on the stator structure is N_r as j and k are any integer numbers. This means that there are N_r radial force wave repetitions in each mechanical cycle. As the mechanical cycle consists of N_r electrical cycles, only one electric cycle is enough to find all the stator force density components in an electric temporal order. The temporal order of the radial force density components based on one electrical cycle is then multiplied by N_r (the number of repetitions in one mechanical cycle) to get the radial force density components represented in the mechanical temporal order.

TABLE 1. Temporal Order of Part of The Radial Force Density Wave Components of a Three-Phase 6/14 SRM.

	J=-4	J=-3	J=-2	J=-1	J=0	J=1	J=2	J=3	GCD
K=-2	-140	-98	-56	-14	28	70	112	154	
K=-1	-154	-112	-70	-28	14	56	98	140	
K=0	-168	-126	-84	-42	0	42	84	126	14
K=1	-182	-140	-98	-56	-14	28	70	112	
K=2	-196	-154	-112	-70	-28	14	56	98	

TABLE 2. Temporal Order of Part of The Radial Force Density Wave Components of a Three-Phase 6/4 SRM.

	J=-4	J=-3	J=-2	J=-1	J=0	J=1	J=2	J=3	GCD
K=-2	-40	-28	-16	-4	8	20	32	44	
K=-1	-44	-32	-20	-8	4	16	28	40	
K=0	-48	-36	-24	-12	0	12	24	36	4
K=1	-52	-40	-28	-16	-4	8	20	32	
K=2	-56	-44	-32	-20	-8	4	16	28	

Table 1 and Table 2 show part of the radial force density wave components of a three-phase 6/14 SRM and a three-phase 6/4 SRM, respectively. As shown in these tables, the GCD of all the mechanical temporal orders is which means that only one electrical cycle is required to find all the radial force density components of SRM if the structure of the machine is symmetric.

B. FRACTION OF AN ELECTRICAL CYCLE METHOD FOR STATOR RADIAL FORCE DENSITY WAVE GENERATION

As discussed in the previous subsection, the stator force density wave based on one electrical cycle of the SRMs FEA simulation can be used to get the accurate stator force density components. That leads to a significant amount of simulation time reduction equal to $(N_r - 1)$ times the computational time of the force density wave calculation based on the FEA simulation of one mechanical cycle.

However, by taking a closer look into the stator radial force density wave, it can be noticed that a further reduction in the required cycles can be achieved. Figure 2 shows a typical electromagnetic radial force density waveform acting on the stator structure of a three-phase 6/4 SRM for one electrical cycle. The electrical cycle in that Figure is divided into 100 rotor positions and the stator circumference, where the radial force density is calculated, is divided into 7770 points for this example. It can be noticed that the waveform is divided into three symmetrical temporal parts that are shifted in the circumferential direction (see Figure.2). These three parts are due to the three-phase machine structure. The number of the symmetrical temporal but shifted parts is equal to the number of machine phases. This means that if only one part is computed, the other two parts can be reproduced by shifting the calculated part in the circumferential direction with a proper shift angle. This assumption is valid

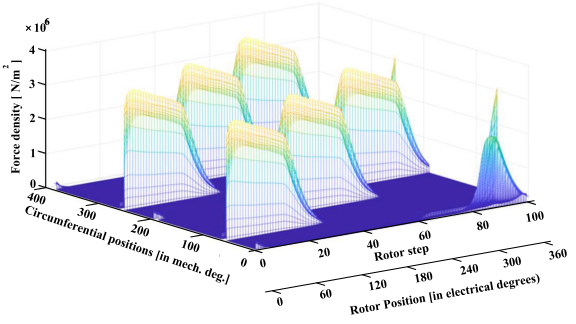

FIGURE 2. A typical radial force density waveform of a three-phase 6/4 SRM over one electric cycle (100 rotor steps) and the whole stator inner circumference.

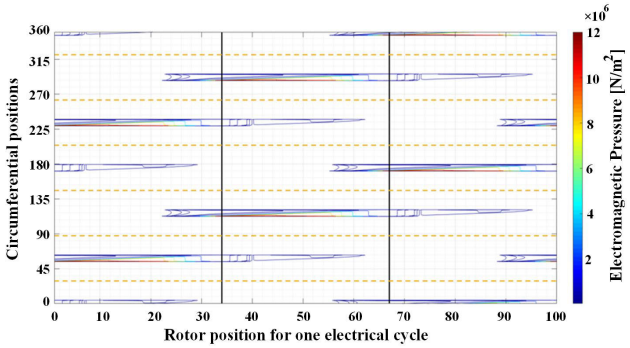

FIGURE 3. A contour plot of the radial force density waveform shown in Figure2.

if the machine structure is symmetrical. The symmetry of the machine is usually the assumption in the machine design stage, so this technique can be used to reduce the time of the design and optimization of the machine as a huge amount of time can be saved.

Figure 3 shows a contour plot of the radial force density wave shown in Figure 2. It is clear from the contour plot that the radial force density wave is divided into three parts, and each part is shifted by a certain mechanical circumferential angle on the stator circumference. To illustrate that, a graphical representation of the radial force density for one electrical cycle of the three-phase 6/4 SRM configuration is presented in Figure 4. The hatched cells in the Figure represent that there is a higher value of the force density at that circumferential position compared to the white cells. The number of hatched cells shown in the Figure indicates the number of the phase excited at the corresponding rotor position. It can be concluded from the contour plot in Figure 3 and the graphical representation in Figure 4 that by moving the excitation from one phase to another phase, the radial force density waveform is shifted circumferentially by 60 mechanical degrees on the stator circumference in the direction of phase excitation or 120 mechanical degrees on the stator circumference in the direction of rotor rotation.

For a three-phase 6/4 SRM, 1/3 of an electrical cycle is required to reproduce the radial force density wave, shown in Figure 5. The other two parts of the radial force density wave can be reproduced by shifting the calculated part by 60 mechanical degrees on the stator circumference in the direction of phases excitation or 120 mechanical degrees on the stator circumference in the direction of rotor rotation, as illustrated in Figure 6. As shown in Figure 6, any three-phase six teeth configuration will require the same shift. The required shift should be changed if the number of stator teeth changes, as shown in Figure 7 for a three-phase with 12 teeth SRM.

The required shift based on the machine slot/pole configuration can be estimated from the following equation:

$$\begin{cases} \theta_{\text{shift}} = \frac{360}{N_s} \text{ in the direction of phase excitation, or} \\ \theta_{\text{shift}} = \frac{360}{N_s}\left(N_{ph} - 1\right) \text{ in the direction of rotation} \end{cases} \quad (2)$$

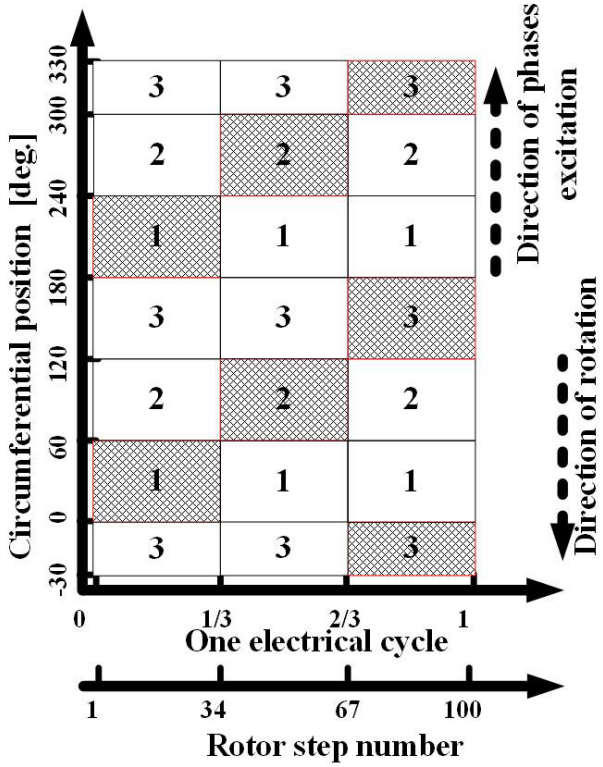

FIGURE 4. A graphical representation of the radial force density waveform regions.

In the simulation of the three-phase 6/4 SRM shown in Figure 2 and Figure 3, the stator inner circumference is divided into 7770 equal-angle points. That means that in order to shift the wave 60 degrees on the stator circumference (in the direction of phase excitation), the 1/3 electrical cycle wave should be shifted 1295 points. The simulated 1/3 electrical cycle wave should be shifted by 2590 points to shift the wave by 120 degrees on the stator circumference. To ensure an integer number results from the shifting process, the stator inner circumference, where the stator force is calculated, should be divided into a number of points equal to $N_r \times N_{ph} \times I$, where I is an integer number.

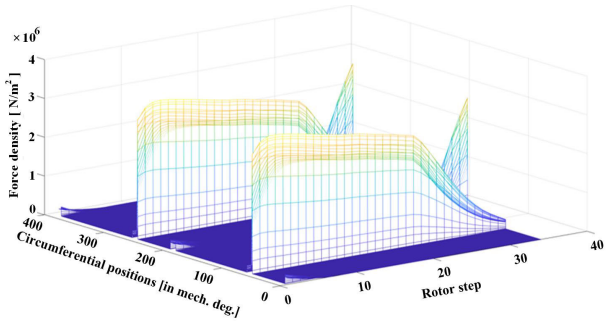

FIGURE 5. The stator radial force density wave of the three-phase 6/4 SRM over 1/3 electric cycle (37 rotor steps).

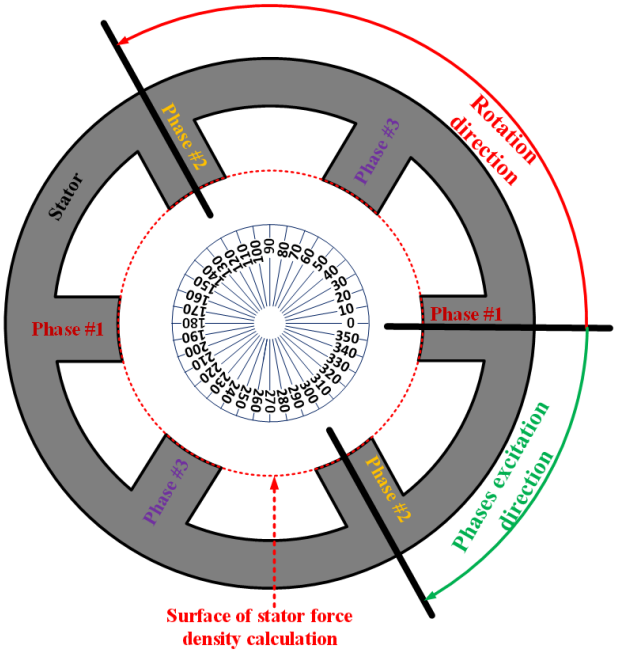

FIGURE 6. Amount of shift applied to regenerate the stator force density for a three-phase with six teeth SRMs configurations (such as 6/14, 6/4 SRMs) Note: phase excitation sequence is (Phase #1, Phase #2, then Phase #3).

Based on this proposed method, the number of FEA simulation points required for obtaining the stator radial force density waves of SRMs is reduced significantly. In general, the stator radial force density wave of a certain SRM configuration can be reproduced by only simulating $1/N_{ph}$ of an electrical cycle of the machine, and the other $(N_{ph}-1)$ parts of the stator radial force density wave can be produced by shifting the calculated part circumferentially with a shift angle θ_{shift} which can be calculated based on (2). Numerical examples to compare the one mechanical cycle method, the one electrical cycle method and the proposed fraction of an electrical cycle method of stator radial force density wave generation and decomposition are presented in section IV.

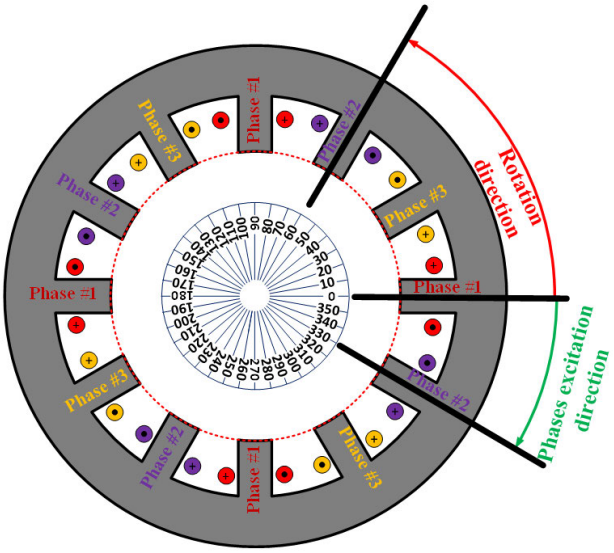

FIGURE 7. Amount of shift applied to regenerate the stator force density for a three-phase with 12 teeth SRMs configurations (such as 12/8 SRMs) Note: phase excitation sequence is (Phase #1, Phase #2, then Phase #3).

III. ROTOR TANGENTIAL FORCE DENSITY CALCULATION DECOMPOSITION

This section discusses the decomposition of the rotor tangential force density and the conventional method to calculate the tangential force density wave. A new method based on a lower number of rotor steps is introduced in this section. The proposed method reduces the FEA simulation time as compared to the conventional method based on one complete mechanical cycle. A computer with Intel(R) Core(TM) i7-8700 CPU @3.20GHz processor and 32.0 GB RAM is used for all the simulations in order to quantify the time reduction with the same computational capability.

A. DECOMPOSING THE ROTOR TANGENTIAL FORCE DENSITY BASED ON ONE FORCE DENSITY WAVEFORM REPETITION SIMULATION

It is clear from the simulation data of SRMs that the torque waveform consists of several strokes in each electric cycle whose number is equal to the number of the machine phases. For example, for the three-phase 6/14 SRM, the number of torque strokes in one electric cycle is 3 (equal to the number of phases), as indicated in Figure 8. If symmetry is considered in the machine design, only one stroke can give accurate information about the mean torque, the torque ripple, and the torque harmonics contents. That means the time of the machine's FE simulation to get the torque information(mean torque, torque ripples) can be decreased $1/N_{ph}$ as compared to the time if one electrical cycle is used.

To prove that the rotor tangential force density wave, which is responsible for the rotor torque production, has been analyzed. The rotor tangential force density harmonics pattern was illustrated in detail in [10] and shown in (3).

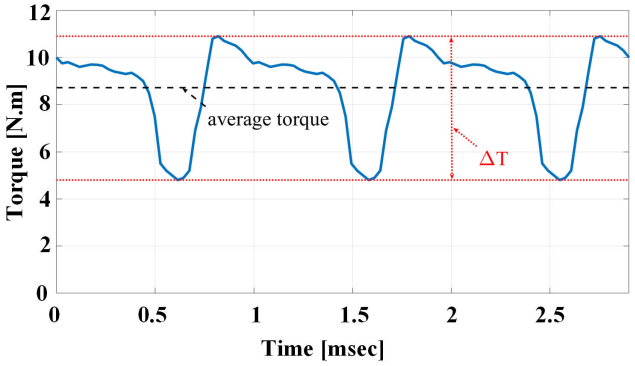

FIGURE 8. A torque waveform of a 6/14 SRM for one electrical cycle.

In (3), u is the temporal order and v is the circumferential order of the force density wave. j and k are integer numbers that are typically used to swipe between the different radial force density harmonics [12].

$$\begin{cases} u = N_r \times N_{ph} \times j - N_s \times k \\ v = \frac{N_s}{N_{ph}} k \end{cases} \tag{3}$$

Table 3 illustrates the temporal order u, of part of rotor tangential force density harmonics pattern for the 6 / 14 SRM configuration based on (3) for different values of j and k.

Based on (3), the torque is calculated for all the wave components to identify the rotor tangential force density components responsible for the torque production. Equation (4) is used to calculate the torque component for any force density component, FD, with temporal order u and circumferential order v [11]:

$$T(u, v) = r \times \int_{\theta=0}^{2\pi} FD(u, v) \times r \times L \times d\theta \tag{4}$$

where r is the rotor radius, L is the rotor stack length, and $d\theta$ is a circumferential increment over the rotor outer circumference.

As the waveform of any force density component is expressed as follows [27], [28]:

$$FD(u, v) = M_{u,v} \cos\left(u\omega t + v\theta + \phi_{u,v}\right) \tag{5}$$

where $M_{u,v}$ is the amplitude of the force density component $\omega = 2\pi f_{\text{mech}}$ is the mechanical angular velocity and $\phi_{u,v}$ is the phase shift of the force density harmonic component.

Based on (4) and (5), Only the force density components with zero circumferential order ($v = 0$) have a torque component. Also, it is clear from these equations that the rotor tangential force density component $FD(u = 0, v = 0)$ is the component responsible for the mean torque production and the radial force density components $FD(u \neq 0, v = 0)$ are responsible for the torque ripples.

The components responsible for the torque harmonics and the mean torque of the 6/14 SRM are the components where $K = 0$ in Table 3. It can be noticed that the GCD of these harmonics is 42, which is $N_r \times N_{ph}$. This implies that there are 42 repetitions in each mechanical cycle, and only one of these

TABLE 3. Temporal Order of Part of The Rotor Tangential Force Density Wave Components of The Three-Phase 6/14 SRM Configuration.

	J=-4	J=-3	J=-2	J=-1	J=0	J=1	J=2	J=3	GCD
K=-2	-156	-114	-72	-30	12	54	96	138	6
K=-1	-162	-120	-78	-36	6	48	90	132	6
K=0	-168	-126	-84	-42	0	42	84	126	42
K=1	-174	-132	-90	-48	-6	36	78	120	6
K=2	-180	-138	-96	-54	-12	30	72	114	6

repetitions is enough to get the mean torque and the torque harmonics for the three-phase 6/14 SRM configuration. This one repetition is $1/N_{ph}$ of an electrical cycle. That can be explained by (3) for any SRM configuration, as the GCD for all the temporal orders with zero circumferential order, $v = 0$, is $N_r \times N_{ph}$. That means there are $N_r \times N_{ph}$ of torque repetitions in one electrical cycle for any SRM configuration. If the machine symmetry holds, only one of these torque repetitions can be used to compute the mean torque and the torque ripple components.

However, if the other circumferential components on the rotor tangential force density where $v \neq 0$ are required, the simulation of $1/N_{ph}$ of an electrical cycle is not sufficient. Based on (3), if all the temporal order harmonics are required with zero and non-zero circumferential orders, the GCD of the temporal order is N_s as N_s is a multiplication of the number of phases (N_{ph}). This means that one electrical cycle ($1/N_r$ of the machine's mechanical cycle) will always be too short or too long compared to the repetition cycle of the machine's rotor tangential force density wave. So, one electrical cycle simulation will be insufficient to get the rotor tangential force density wave components.

For example, for the three-phase 6/14 SRM, the rotor tangential force density wave resulting from the FE simulation of one electrical cycle is insufficient for calculating the rotor tangential force density components as 1/6 of the mechanical cycle is needed to be simulated, which corresponds to 14/6 electric cycles.

Figure 9 shows a graphical representation of the number of tangential force density repetitions and the number of electrical cycles within on mechanical cycle for three different SRM configurations. For example, one mechanical cycle of a three-phase 6/4 SRM has six repetitions of the rotor tangential forces density wave and has four electrical cycles. This means that the rotor radial force density wave decomposition performed on one electrical cycle may be insufficient for the rotor tangential force spectrum. Only 2/3 (N_r/N_s) of an electrical cycle is sufficient to get the force spectrum in a hypothetical temporal order. The force wave spectrum can be represented after that in the mechanical temporal by multiplying the hypothetical temporal orders of the spectrum by 6 (N_s), which is the number of tangential force density wave repetitions in one mechanical cycle.

In general, the number of parts of the mechanical cycle required to get the accurate rotor force density component

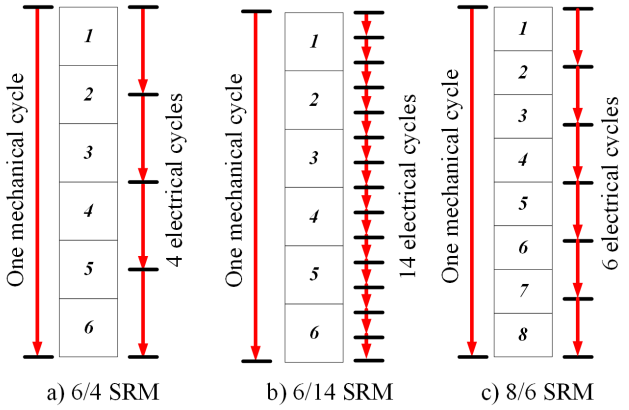

FIGURE 9. A graphical representation of the tangential force repetition within a complete mechanical cycle for three different configurations: a) three-phase 6/4SRM, b) three-phase 6/14 SRM, and c) four-phase 8/6 SRM.

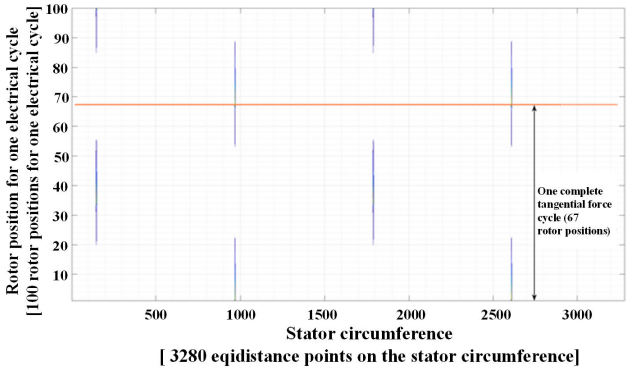

FIGURE 10. The contour plot of the tangential force density of a 6/4 SRM rotor over the complete circumference of the rotor and for a complete electrical cycle.

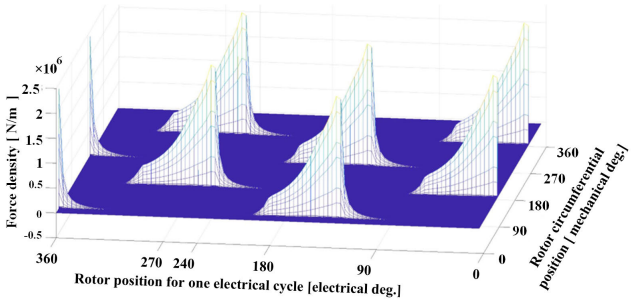

FIGURE 11. The rotor tangential force of a 6/4 SRM for one electrical cycle.

can be obtained from the following equation:

$$C_{\text{parts}} = \frac{1}{N_s}, \tag{6}$$

and the corresponding number of electrical cycles to get the accurate rotor force density spectrum is given by:

$$C_{\text{elec}} = \frac{N_r}{N_s}. \tag{7}$$

The 2/3 of an electrical cycle of the three-phase 6/4 SRM represents exciting the machine for 240 degrees electrical angle. The same results should be obtained if one mechanical cycle is simulated, but the mechanical order will represent the temporal order.

A three-phase 6/4 SRM was simulated for a complete electrical cycle. As shown in Figure 10, only 2/3 of the electrical cycle (67 rotor steps out of 100 steps) has a complete rotor tangential force density wave. That cycle can be used to get the machine's rotor tangential force density harmonics. As shown in Figure 11, the rotor tangential force is repeated after 240 electrical degrees (2/3 of an electrical cycle). If a complete electrical cycle is used, the force component resulting from the FFT decomposition will not be accurate as compared to the one obtained by one mechanical cycle and the one tangential density wave repetition.

Applying the same principle on a three-phase 6/14 SRM and a four-phase 8/6 SRM, the rotor tangential force density components should be calculated for 840 electrical degrees and 270 electrical degrees, respectively. Theoretically, this method can be generalized for any SRM as follows:

$$\theta_{\text{elec}} = C_{\text{elec}} * 360 \tag{8}$$

where θ_{elec} is the rotor position period in electrical degrees required to be simulated to generate one complete rotor tangential force density on the SRM repetition.

For the four-phase 8/6 SRM, 3/4 of an electrical cycle is required to get the accurate frequency spectrum of the machine's rotor tangential force density wave, as indicated in (7) and Figure 9.c. The force spectrum will be in the exact spatial order of the machine but in a hypothetical temporal order. The hypothetical temporal order is then multiplied by N_s, as indicated before, to represent the force spectrum in the mechanical temporal order. The 3/4 of an electrical cycle simulation of the four-phase 8/6 SRM means the machine should be simulated for 270 electrical degrees. This means that one electrical cycle is too long, and if the tangential force density wave of one electrical cycle is used for the decomposition process, the results will not be accurate and not represents the actual rotor tangential force density harmonics.

The case of a three-phase 6/14 SRM is, however, different. One full electric cycle is too short to get an accurate rotor tangential force density spectrum, as shown in the graphical representation in Figure 9.b. The 6/14 SRM requires 7/3 electrical cycles to get the correct frequency spectrum of the rotor force components, as indicated in (7). In other words, the machine should be simulated for 840 electrical degrees to get the correct rotor tangential force density spectrum in a hypothetical temporal order. The hypothetical temporal order should then be multiplied by 6 (the number of force repetitions in one mechanical cycle, N_s) to get the force components in the machine's mechanical temporal order.

B. FRACTION OF AN ELECTRICAL CYCLE METHOD FOR ROTOR TANGENTIAL FORCE DENSITY WAVE GENERATION

In this subsection, a new method is applied to regenerate a complete rotor tangential force density cycle based on the simulation of $1/N_{ph}$ of an electrical cycle. That means reducing the force calculation time significantly. For example, the time required to obtain the rotor tangential force density wave with the new method for a three-phase 6/4SRM is reduced by half for a three-phase 6/14SRM, the time is reduced by 6/7, and for a four-phase 8/6 SRM, the time is reduced by 2/3 of the time used to obtain the rotor tangential force density wave based on one rotor tangential wave repetition.

In the proposed method, the rotor tangential force density information is estimated based on the simulation of $1/N_{ph}$ of an electrical cycle. Like the reduced data method used for the stator force density regeneration indicated in section II, the rotor force density data based on $1/N_{ph}$ is shifted circumferentially on the rotor circumference with a certain shift angle to construct the remaining force density parts to complete a full rotor force density wave.

Based on (7), The minimum number of electrical cycles required to decompose the rotor tangential force density of an SRM is N_r/N_s electrical cycles. It was found by simulation that each rotor tangential force density repetition cycle consists of an N_{ph} number of identical but shifted parts. As shown in Figure 10 and Figure 11, the one rotor tangential force density waveform (2/3 of an electrical cycle) of the three-phase 6/4 SRM consists of two identical but circumferentially shifted parts. This implies that each complete rotor tangential force repetition consists of $N_{ph} * N_r/N_s$ identical but shifted parts. So, if only one of these parts is simulated and the proper circumferential shift angle is applied, the other parts can be regenerated, and the simulation time will be reduced significantly. This condition holds only if the design of the machine is symmetrical.

The rotor tangential force density of different SRM configurations is simulated, and graphical representations that show the tangential force density distribution on the rotor circumference are illustrated in this section. As shown in Figure 12, For the three-phase 6/14SRM, if $1/N_{ph}$ of the electrical cycle is simulated, the full wave tangential force density could be regenerated by post-processing of the FEA simulation results by shifting the generated waveform by 77.1429 degrees mechanical on the circumferential direction opposite to the direction of rotation. The number of cells in one column of Figure 12 indicates the number of rotor teeth. Seven columns represent the number of identical but shifted parts in one repetition cycle of the machine's rotor tangential force density wave. The hatched cells in Figure 12 indicate where the rotor tangential force has a larger value than white cells. They correspond to rotor teeth facing excited stator teeth. Only one part is simulated, and the other six parts of the tangential force density wave can be regenerated by shifting. That means the method can be used to reduce the simulation time required to obtain the rotor tangential force density wave

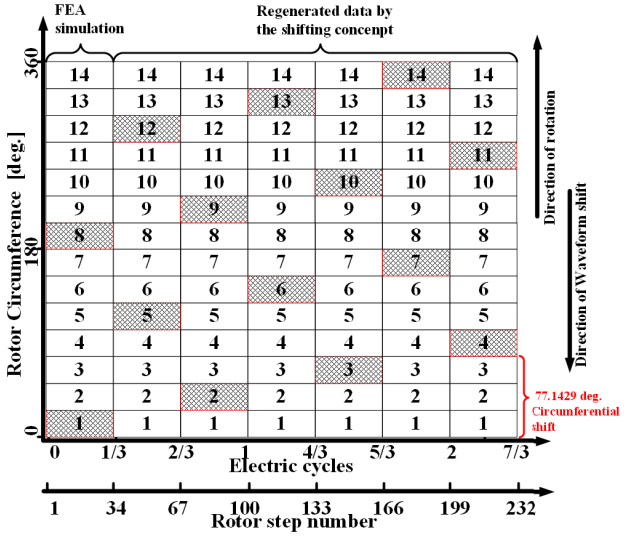

FIGURE 12. An illustrative diagram showing the regeneration process of a complete rotor tangential force density cycle of a three-phase 6/14 based on 1/3 electrical cycle FEA simulation.

by 6/7 times the time required for the one repetition method introduced in this section.

As shown in the illustrative diagram in Figure 13, For a three-phase 12/16 SRM, only $1/3\,(1/N_{ph})$ of the electrical cycle is required to be simulated to regenerate the rest of the tangential force density wave parts. The simulation data show that for the three-phase 12/16 SRM the circumferential shift angle to generate the full rotor tangential force density wave out of 1/3 of an electrical cycle is 67.5 mechanical degrees in the circumferential direction opposite to the direction of rotation. Equation (9) is developed to calculate the circumferential shift angle needed to generate the full rotor tangential force density based on the simulation of $1/N_{ph}$ of an electrical cycle for an N_s/N_r SRM configuration with N_{ph} number of phases:

$$\theta_{\text{shift}} = \text{roundup}\left(\frac{N_r}{N_s} * \frac{\theta_{\text{excitation}}}{360/N_s}\right) * \frac{360}{N_r} \tag{9}$$

where $\theta_{\text{excitation}}$ is the mechanical angle between two successive excited phases in the opposite direction of the rotor rotation. For example, $\theta_{\text{excitation}} = 60°$ for the three-phase 6/14 SRM configuration. The number of rotor tangential force density parts needed to be regenerated after the FEA simulation of $1/N_{ph}$ of an electrical cycle is given as follows:

$$R_{\text{parts}} = \left(\frac{N_r N_{ph}}{N_s} - 1\right) \tag{10}$$

The circumferential shift angle to generate the full rotor tangential force density of a three-phase 12/8 SRM, a five-phase 10/14 SRM, a four-phase 8/6 SRM, and a three-phase 6/4 SRM configurations are shown in Figure 14, Figure 15, and Figure 16, respectively. The circumferential shift angle and the number of parts needed to be generated for all of the mentioned configurations are summarized in Table 4.

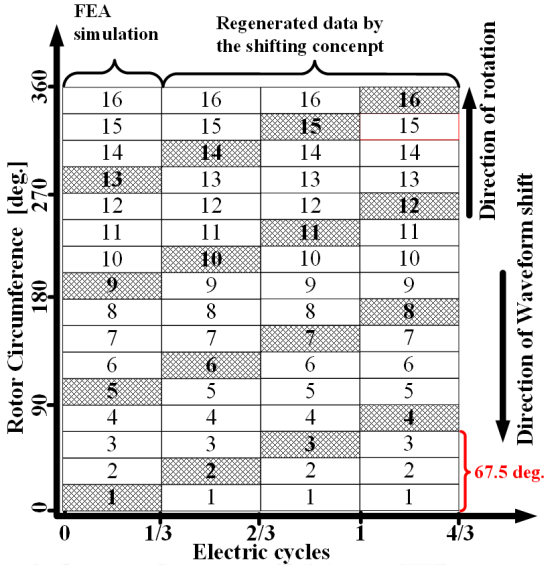

FIGURE 13. An illustrative diagram showing the regeneration process of a complete rotor tangential force density cycle of a Three-phase 12/16 based on 1/3 electrical cycle FEA simulation.

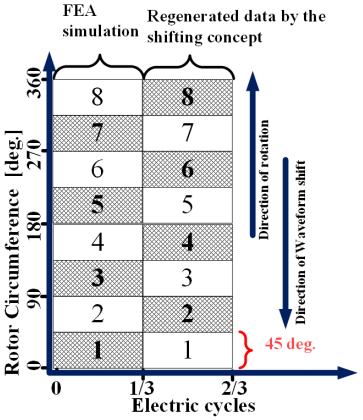

FIGURE 14. An illustrative diagram showing the regeneration process of a complete rotor tangential force density cycle of a Three-phase 12/8 based on 1/3 electrical cycle FEA simulation.

The method results in a considerable time reduction as compared to the time required for obtaining one cycle of the rotor tangential force with the one repetition method illustrated before in this section. The time saved by using a fraction of an electrical cycle method compared to the one tangential force density wave repetition method depends on the machine number of rotor teeth, stator teeth and phases. In general, the percentage of time reduction using this method compared to the one tangential force density repetition is given by the formula:

$$\text{Time reduction } \% = \left(\frac{N_r N_{ph} - GCD\left(N_r N_{ph}, N_s\right)}{N_r N_{ph}} \right) * 100\% \qquad (11)$$

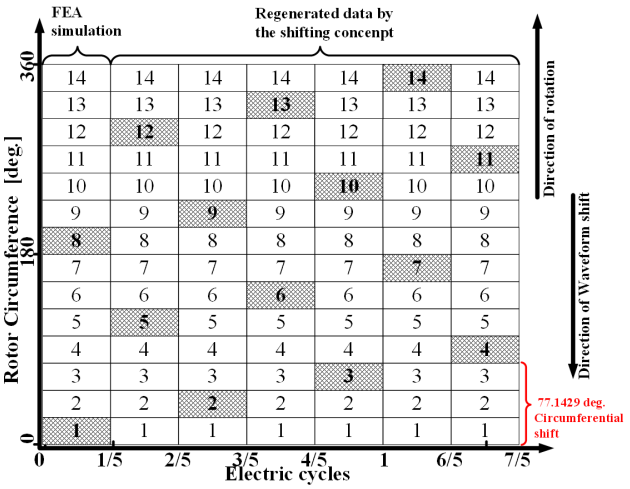

FIGURE 15. An illustrative diagram showing the regeneration process of a complete rotor tangential force density cycle of a five-phase 10/14 based on 1/5 electrical cycle FEA simulation.

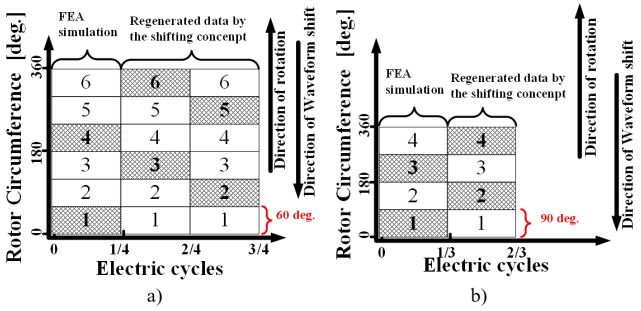

FIGURE 16. An illustrative diagram showing the regeneration process of a complete rotor tangential force density cycle of two SRMs configurations: a) a four-phase 8/6 SRM configuration and b) a three-phase 6/4.

IV. NUMERICAL EXAMPLES OF STATOR RADIAL FORCE DENSITY WAVES GENERATION AND DECOMPOSITION METHODS

In this section, the complete radial force density wave is simulated for one mechanical cycle and one electrical cycle and regenerated using a fraction of an electrical cycle method by the FE simulation of $1/N_{ph}$ of an electrical cycle. The radial force density waves of three different SRM configurations are obtained based on the three methods and then decomposed with a two-dimensional fast Fourier transform (2D FFT) to calculate the stator radial force density harmonic spectrum. The harmonic spectrum based on one electrical cycle and the reduced data method introduced in this paper is compared to the harmonic spectrum based on the simulation of one mechanical cycle as a benchmark method.

A. NUMERICAL EXAMPLES OF USING ONE ELECTRICAL CYCLE AND ONE MECHANICAL CYCLE

The radial force density waves for three different configurations of SRMs, three-phase 6/4 SRM, three-phase 6/14 SRM, and four-phase 8/6 SRM, are calculated based on the

TABLE 4. Example of the FEA simulation period, the mechanical shift, and the number of regenerated parts of the rotor tangential force density wave required for different SRMs configurations.

SRM configuration	FEA simulation period required	Mechanical shift angle	Number of regenerated parts
Three-phase 6/4	1/3 of an electrical cycle	90	1
Three-phase 6/14	1/3 of an electrical cycle	77.1429	6
Three-phase 12/8	1/3 of an electrical cycle	45	1
Three-phase 12/16*	1/3 of an electrical cycle	67.5	3
Four-phase 8/6	1/4 of an electrical cycle	60	2
Five-phase 10/14**	1/5 of an electrical cycle	77.1429	5

* The firing sequence in this analysis for the three-phase 12/16 SRMs configuration is assumed to be Ph#1 – Ph#2 – Ph#3 – Ph#1, so the angle between two successive excited phases in the opposite direction of rotor rotation is 60deg.
** The firing sequence in this analysis for the five-phase 10/14 SRMs configuration is assumed to be Ph#1 – Ph#3 – Ph#5 – Ph#2– Ph#4 – Ph#1, so the angle between two successive excited phases in the opposite direction of the rotor is 72deg.

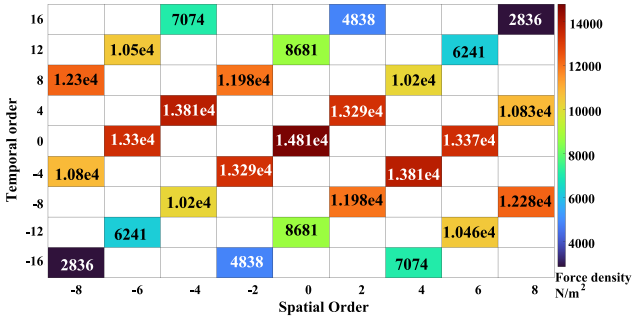

FIGURE 17. The radial force density of a 6/4 SRM based on a complete mechanical cycle.

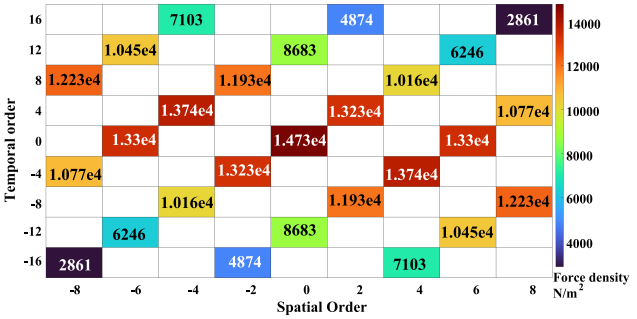

FIGURE 18. The radial force density on the stator of a 6/4 SRM based on a complete electrical cycle.

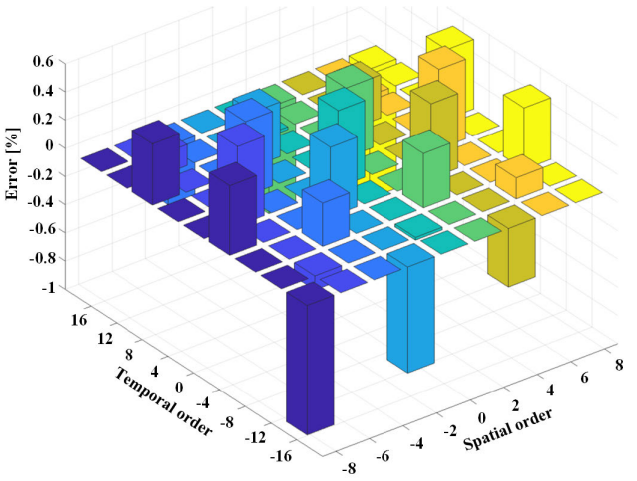

FIGURE 19. The error of stator radial force density spectrum calculated based on the one electrical cycle method with respect to the spectrum calculated based on the one mechanical cycle method for the case study three-phase 6/4 SRM.

simulation of one complete mechanical cycle and one complete electrical cycle to evaluate the effectiveness of using one electrical cycle to get all the radial force density wave components.

The radial force density wave of a 6/4 SRM is obtained based on one mechanical cycle and one electrical cycle. The two radial force density waves based on the two methods are then decomposed to the wave components with 2D FFT decomposition. After obtaining the radial force density spectrum based on the one electrical cycle method, the temporal order of the spectrum is multiplied by 6 (the number of rotor teeth) to represent the spectrum in the mechanical temporal order, as illustrated in section II. The stator radial force density waves harmonics spectrum for the one mechanical cycle method and the one electrical cycle method are presented in Figure 17 and Figure 18, respectively.

The relative error of the stator radial force density harmonics spectrum calculated based on the one electrical cycle method with respect to the spectrum calculated based on the one mechanical cycle method is shown in Figure 19. It can be noticed that one electrical cycle can be effectively used for the decomposition of the radial force density components of the 6/4 SRM to get its harmonics spectrum with a reduced simulation time and simulation effort. Figure 19 shows that the maximum error between the two methods for the displayed spectrum is less than 1%.

Figure 20 shows the stator radial force density harmonics spectrum of a three-phase 6/14 SRM calculated based on the FEA simulation of one mechanical cycle. The one electrical cycle method is then used to obtain the radial force density spectrum of that machine. The error of the stator radial force density harmonics spectrum calculated based on the one electrical cycle method with respect to the spectrum calculated based on the one mechanical cycle method is then calculated (see Figure 21). As shown in Figure 21, the maximum error of the radial force density based on the one electric cycle method with respect to one mechanical cycle method for the

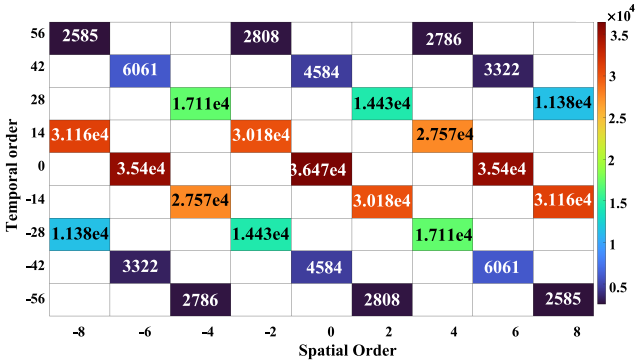

FIGURE 20. The stator radial force density components of a 6/14 SRM based on a complete mechanical cycle.

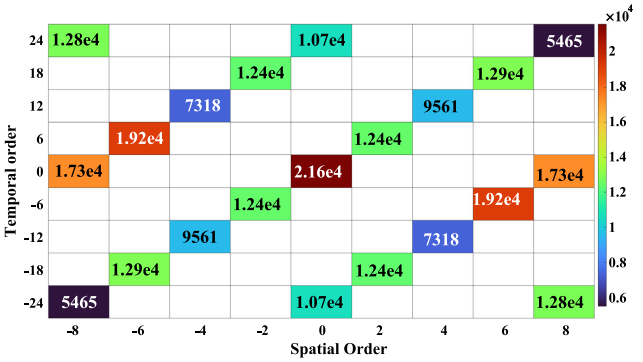

FIGURE 22. The stator radial force density components of a four-phase 8/6 SRM based on a complete mechanical cycle.

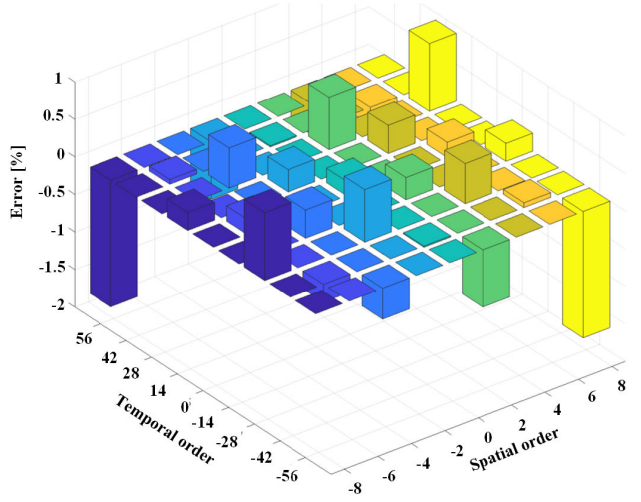

FIGURE 21. The error of stator radial force density spectrum calculated based on the one electrical cycle method with respect to the spectrum calculated based on the one mechanical cycle method for the case study three-phase 6/14 SRM.

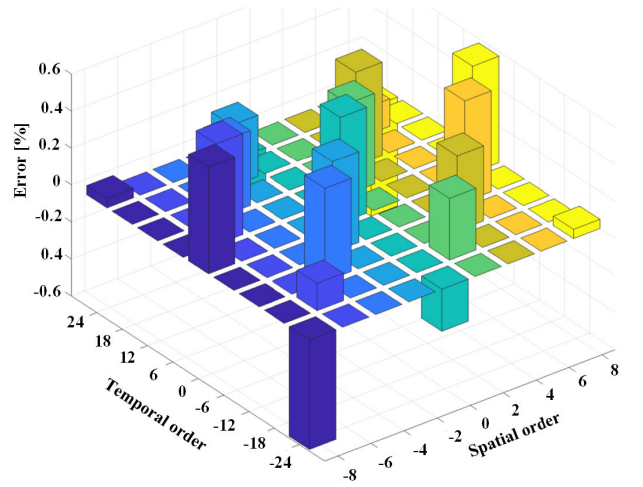

FIGURE 23. The error of stator radial force density spectrum calculated based on the one electrical cycle method with respect to the spectrum calculated based on the one mechanical cycle method for the case study four-phase 8/6 SRM.

case study three-phase 6/14 SRM on the displayed spectrum is about 1.8%.

The stator radial force density waveform is obtained for a third case study, four-phase 8/6 SRM, based on the simulation of one mechanical cycle and then the waveform is decomposed to the harmonic spectrum as shown in Figure 22. Using the one electrical cycle method, the stator radial force density harmonics spectrum is calculated. The error of the stator radial force density harmonics spectrum calculated based on the one electrical cycle method with respect to the spectrum calculated based on the one mechanical cycle method is then calculated as presented in Figure 23. As shown in Figure 23, the maximum error of the radial force density spectrum calculated based on the case study four-phase 8/6 SRM is less than 0.6%.

B. USING THE PROPOSED APPROACH FOR STATOR RADIAL FORCE DENSITY REGENERATION AND DECOMPOSITION

The stator radial force density waves for the three case studies SRM configurations mentioned before are regenerated based on the fractional of an electrical cycle method introduced in section II. The regenerated stator radial force density waves for the three configurations are then decomposed into the radial force density harmonics spectrum, and the error is calculated with respect to the stator radial force density spectrum calculated based on the one mechanical cycle benchmark method.

A faction of an electrical cycle method is used to regenerate the stator radial force density wave for a three-phase 6/4 SRM. As indicated in section II, for the three-phase 6/4 SRM, only 1/3 of an electrical cycle is sufficient to generate one repetition of the stator radial force density wave. The three-phase 6/4 SRM is simulated for 1/3 of an electrical cycle (37 rotor steps are used in the simulation), as shown in Figure 5. Then, one electrical cycle of the stator radial force density of the machine is generated based on the simulated part of the stator radial force density wave by shifting that part of the wave (see Figure 5) two times by 60 degrees mechanically on the stator circumference in the opposite direction to the rotor rotation. The regenerated wave

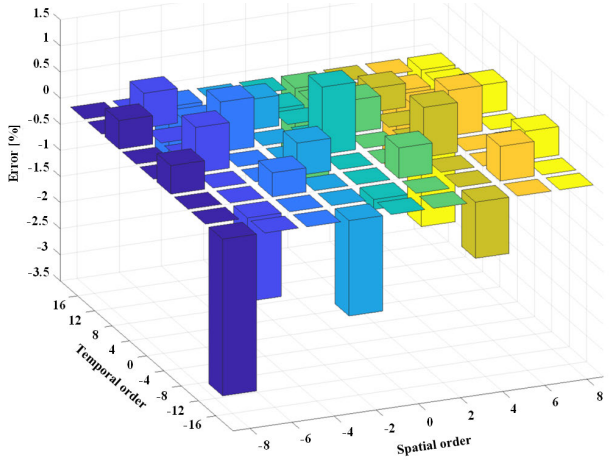

FIGURE 24. The radial force density on the stator of a 6/4 SRM based on the data of 1/3 of an electrical cycle.

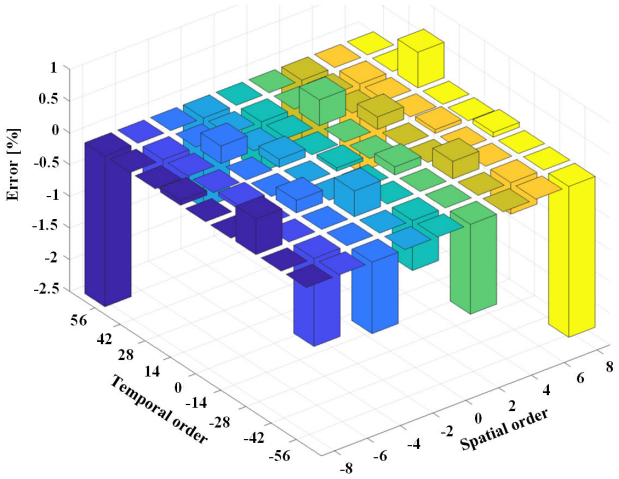

FIGURE 25. The radial force density on the stator of a 6/14 SRM based on the data of 1/3 of an electrical cycle.

TABLE 5. A comparison of the simulation time required and the maximum error for obtaining the stator radial force density wave spectrum of the case study three-phase 6/4 SRM for the three methods discussed in the paper.

	Based on one mechanical cycle (4 electrical cycles)	Based on one radial force repetition (One electrical cycle)	Fractional of an electrical cycle method (1/3 electrical cycle)
Time used FEA simulation for Force Calculation	12 p.u.	3 p.u.	1 p.u.
Maximum error in the displayed spectrum	0%	$< 1\%$	$< 3.5\%$

TABLE 6. A comparison of the simulation time required and the maximum error for obtaining the stator radial force density wave spectrum of the case study three-phase 6/14 SRM for the three methods discussed in the paper.

	Based on one mechanical cycle (14 electrical cycles)	Based on one radial force repetition (One electrical cycle)	Fractional of an electrical cycle method (1/3 electrical cycle)
Time used FEA simulation for Force Calculation	42 p.u.	3 p.u.	1 p.u.
Maximum error in the displayed spectrum	0%	$< 1.8\%$	$< 2.5\%$

represents one electrical cycle of the stator radial force density wave. The wave is then decomposed using 2D FFT, and the error is calculated for the stator radial force density spectrum estimated based on the proposed method with respect to the spectrum obtained by the benchmark one mechanical cycle method shown in Figure 17. As indicated in Figure 24, the maximum error of the displayed force spectrum for a fraction of an electrical cycle method for the three-phase 6/4 SRM is less than 3.5%.

For the three-phase 6/4 SRM, the fractional of an electrical cycle method requires simulating the machine for 1/3 of an electrical cycle; however, the electrical cycle method requires the simulation of one electrical cycle, and the one mechanical cycle method requires the simulation of 4 electrical cycles. For the fractional cycle method, the machine is simulated for 34 rotor steps; however, the machine is simulated for 100 rotor positions for the one electrical cycle method and 397 rotor positions for the one mechanical cycle method. So, it is also clear that the calculation time required for the proposed method is 1/12 the time required for the one mechanical cycle method and 1/3 the time required for one electrical cycle method. Table 5 summarizes the comparison of the three methods for obtaining the stator radial force density wave components for the case study three-phase 6/4 SRM. The table shows the FEA simulation time and the maximum error in the displayed spectrum with respect to the one mechanical cycle benchmark method.

The proposed method is used to generate the stator radial force density wave for the case study three-phase 6/14 SRM. For the case study three-phase 6/14 SRM, the maximum error of the method of fractional of an electrical cycle is less than 2.5% compared to the one mechanical cycle benchmark method, as illustrated in Figure 25.

The proposed method for calculating the stator radial force density wave and its components reduces the calculation FEA simulation computational burden and time to (1/42) of the time required for the complete mechanical cycle method with a maximum error of less than 2.5%. Also, the method reduces the FEA simulation time and computational burden requirements to (1/3) of that of the one electrical cycle method. The summary of the FEA simulation time and the maximum error for each method with respect to the benchmark one mechanical cycle method in the displayed spectrum is summarized in Table 6.

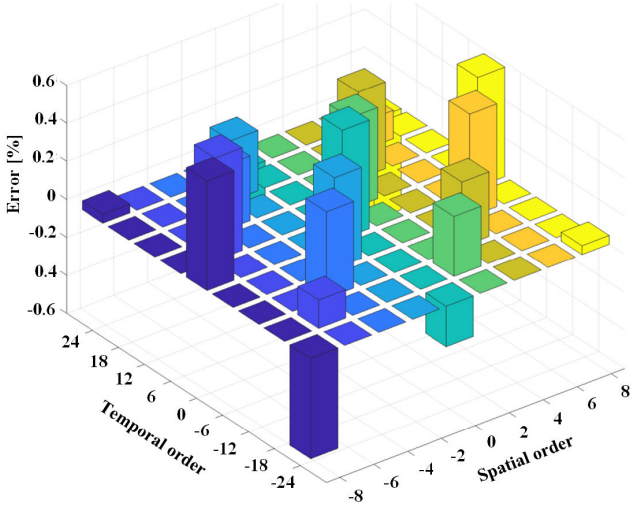

FIGURE 26. The radial force density on the stator of a four-phase 8/6 SRM based on the data of 1/4 of an electrical cycle.

The method is also used to generate the stator radial force density wave for the case study four-phase 8/6 SRM. For the case study machine, the maximum error of the method of fractional of an electrical cycle is less than 0.6% compared to the one mechanical cycle benchmark method, as illustrated in Figure 26.

As indicated in section II, the proposed method only required the machine to be simulated for 1/4 of an electrical cycle for the four-phase 8/6 SRM. The FEA simulation time and the maximum error for each method with respect to the benchmark one mechanical cycle method in the displayed spectrum are summarized in Table 7.

V. NUMERICAL EXAMPLES OF ROTOR TANGENTIAL FORCE DENSITY WAVES GENERATION AND DECOMPOSITION METHODS

The rotor tangential force density wave of three different SRM configurations, three-phase 6/4 SRM, three-phase 6/14 SRM, and four-phase 8/6 SRM, are obtained based on the three different methods mentioned in this paper and then decomposed with 2D FFT to the rotor tangential force density harmonic spectrum for comparison. The harmonic spectrum based on the one-rotor tangential force repetition method and the reduced data method introduced in this paper is compared to the harmonic spectrum based on one mechanical cycle as a benchmark.

The error of the force calculation should be as minimum as possible. If the error of the force calculation is relatively high, this will possibly lead to the convergence to a non-optimal solution during the optimization process. It can be seen in the paper that the new proposed method results in a higher calculation error compared to the one electrical cycle method; however, the increase in the error is not significant as shown in Table 5, Table 6, and Table 7. The new method has the advantage of reducing the calculation time of the force density wave at the cost of a small increase in the calculation error.

TABLE 7. A comparison of the simulation time required and the maximum error for obtaining the stator radial force density wave spectrum of the case study four-phase 8/6 SRM for the three methods discussed in the paper.

	Based on one mechanical cycle (6 electrical cycles)	Based on one radial force repetition (One electrical cycle)	Fractional of an electrical cycle method (1/4 electrical cycle)
Time used FEA simulation for Force Calculation	24 p.u.	4 p.u.	1 p.u.
Maximum error in the displayed spectrum	0%	$< 0.6\%$	$< 0.6\%$

A. NUMERICAL EXAMPLES OF USING ONE TANGENTIAL FORCE REPETITION AND ONE MECHANICAL CYCLE METHODS

The rotor tangential force density wave of the case study 6/4 SRM is obtained based on the FEA simulation of one mechanical cycle of the machine. The rotor tangential force density wave is then decomposed to the wave components based on the 2D FFT as presented in Figure 27. The rotor tangential force density wave is then obtained by only simulating the machine for 2/3 of an electrical cycle (240 electrical degrees) as illustrated in section III and presented in the contour plot in Figure 10 and the force density wave in Figure 11. The rotor tangential force density wave simulated based on the one tangential force repetition method is then decomposed to its components as presented in Figure 28.

The one mechanical cycle method is considered to be the benchmark for the calculation of the error for the proposed methods for obtaining the rotor tangential force density components. The error is calculated for the rotor tangential force density wave harmonics spectrum obtained by using the tangential force repetition cycle method with respect to the spectrum obtained by using the one mechanical cycle method. As presented in Figure 29, the maximum error of the one tangential force repetition method is less than 4% for the displayed spectrum.

The one mechanical cycle method is used to obtain the rotor tangential force density wave of a case study three phase 6/14 SRM. The rotor tangential force density wave is then decomposed to the wave components using 2D FFT analysis. The rotor tangential force density wave components based on the one mechanical cycle method are presented in Figure 30. The one mechanical cycle method required the FE simulation of the machine for 14 electrical cycles. The one-rotor tangential force repetition is then used to obtain the rotor tangential force density components. According to the method introduced in the paper and using (7), the machine is simulated for a 7/3 electrical cycle. The rotor tangential force

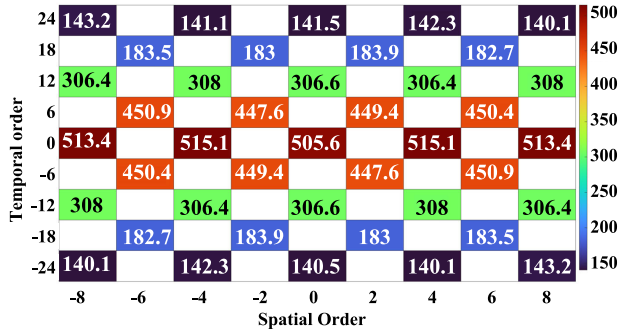

FIGURE 27. The rotor tangential force density components of 6/4 SRM based on the force information of one mechanical cycle.

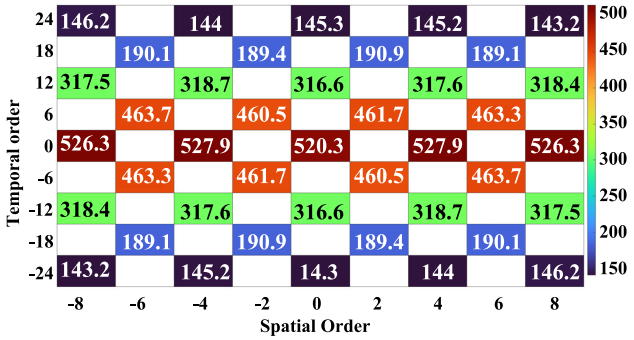

FIGURE 28. The rotor tangential force density components of the case study three-phase 6/4 SRM based on the force information of one rotor tangential force repetition method.

density wave obtained by the method is then decomposed by 2D FFT analysis to the rotor tangential force density components. The error is calculated for the rotor tangential force density wave harmonics spectrum obtained using the rotor tangential force repetition method with respect to the spectrum obtained using the one mechanical cycle method. As presented in Figure 31, the maximum error of the one tangential force repetition method is about 0.458% for the displayed spectrum.

The one mechanical cycle method is used to obtain the rotor tangential force density wave of a third case study machine, a four-phase 8/6 SRM. The obtained waveform is then decomposed using 2D FFT to get the rotor tangential force density components (see Figure 32). The method required the FE simulation of the machine for six electric cycles. However, the rotor tangential force density repetition cycle method requires the machine to be simulated for 6/8 of an electrical cycle (270 degrees electrically), as given by (7). The machine is simulated for 6/8 of an electrical cycle, and the resulting rotor tangential waveform is decomposed to its components. The error is calculated for the tangential force density waveform harmonics spectrum calculated based on the one rotor tangential force density repetition method with respect to the spectrum calculated based on the one mechanical cycle method as presented in Figure 33. As illustrated in Figure 33, the maximum error of using the one rotor

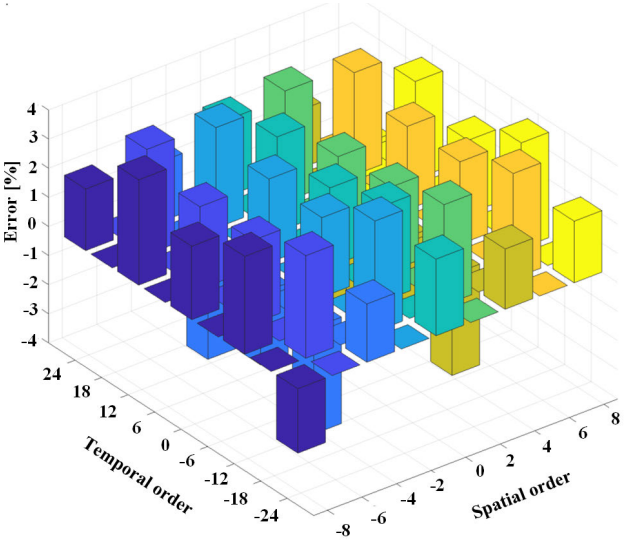

FIGURE 29. The percentage error spectrum of the rotor tangential force density wave obtained by the one tangential force repetition method with respect to the spectrum obtained by the one mechanical cycle method for the case study three-phase 6/4 SRM.

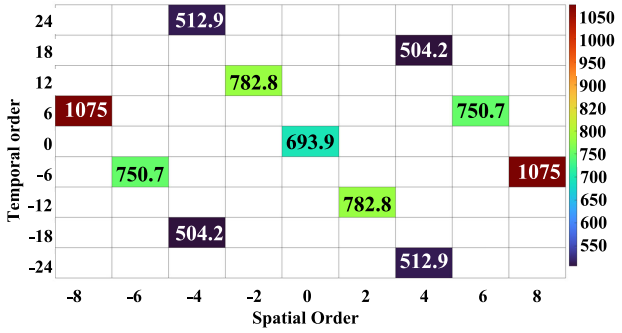

FIGURE 30. The rotor tangential force density components of the case study three-phase 6/14 SRM based on the one mechanical cycle method.

tangential force wave repetition method is about 0.963%. That shows the effectiveness of using the one-rotor tangential force repetition method for the tangential force density evaluation and saving computational time and effort with the proposed method.

B. NUMERICAL EXAMPLES OF USING ONE FRACTIONAL OF AN ELECTRICAL CYCLE METHOD FOR ROTOR FORCE GENERATION AND DECOMPOSITION

The proposed method in section III is used to generate a one-rotor tangential force density repetition of the case study three-phase 6/4 SRM. The machine is simulated for 1/3 of an electrical cycle, and the resultant rotor tangential force density wave is shifted one time by 90 mechanical degrees in the opposite direction of rotor rotation, as indicated in Figure 16.b. The one-repetition rotor force density wave resulting from this process is then decomposed into the force density components. The error of the rotor force density wave components obtained based on the fractional of an

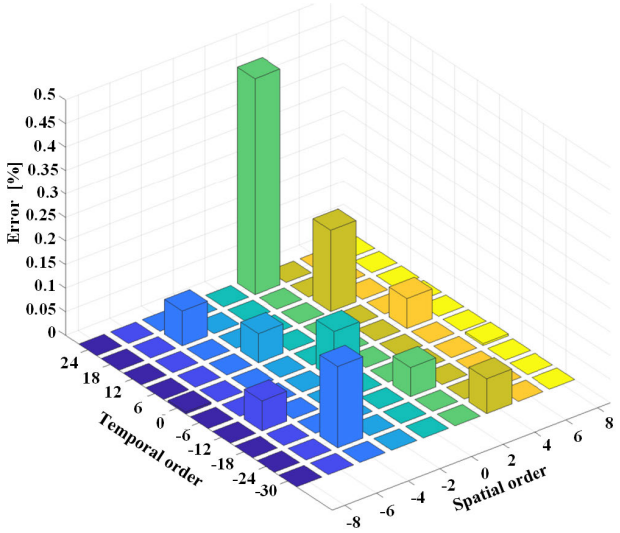

FIGURE 31. The rotor tangential force density components of a 6/14 SRM based on one radial force repetition (840 electrical degrees) represented in the mechanical temporal order.

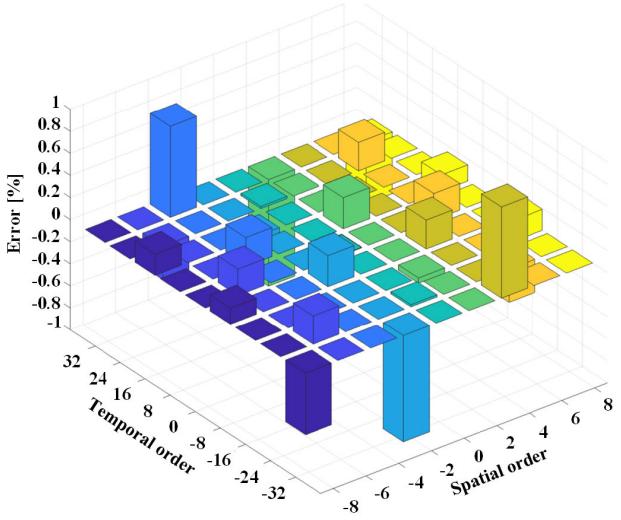

FIGURE 33. The rotor tangential force density components of a four-phase 8/6 SRM based on one radial force repetition (270 electrical degrees) represented in the mechanical temporal order.

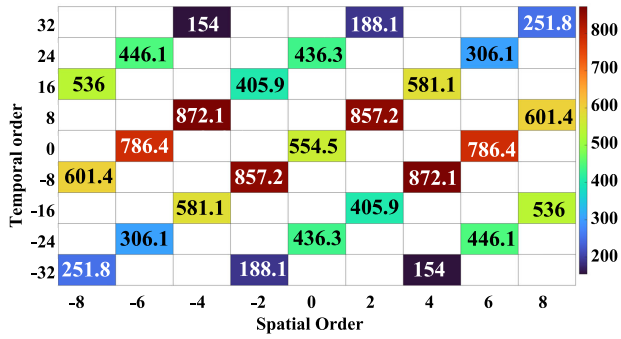

FIGURE 32. Rotor tangential force density components of a four-phase 8/6 SRM based on one mechanical cycle simulation (2160 electrical degrees) represented in the mechanical temporal order.

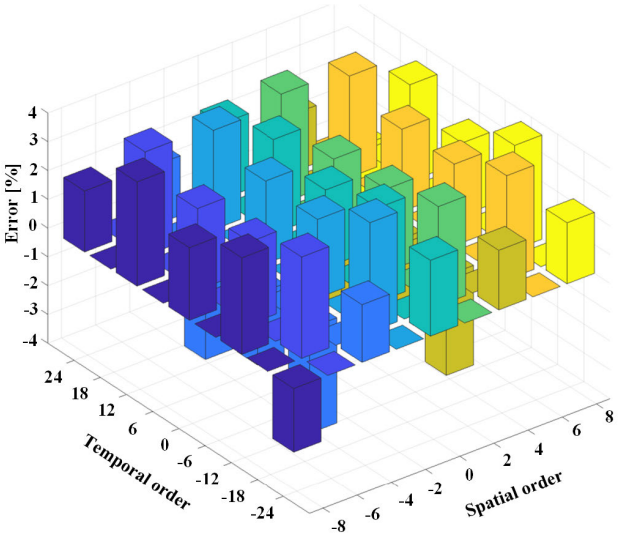

FIGURE 34. The rotor tangential force density components of the 6/4 SRM based on the reproduced force information for one force repetition.

electrical cycle method is calculated with respect to rotor force density components of the machine obtained based on the one mechanical cycle method (see Figure 34). As shown in Figure 34, the maximum error of the fractional of an electrical cycle method with respect to the one mechanical cycle method for obtaining the rotor tangential force density components of the case study three-phase 6/4 SRM is less than 4%. Table 8 shows a comparison between FE simulation time and the maximum error for the three methods used in this paper to obtain the rotor tangential force density components. The error is calculated with respect to the results of the one mechanical cycle method. As indicated by the table, the proposed rotor tangential force repetition method reduced the calculation time by five times, and the proposed fractional of an electrical cycle method reduced the calculation time by ten times compared to the time required for the one mechanical cycle method. The maximum error observed for the displayed spectrum of rotor tangential force density of the case study three-phase 6/4 SRM configuration is less than 4% for both proposed methods compared to the one mechanical cycle method.

The fractional of an electrical cycle method is used to generate the rotor tangential force density wave of the case study three-phase 6/14 SRM. As indicated in Figure 12, only 1/3 of an electrical cycle can be simulated, and the produced rotor tangential force density wave can be shifted six times in the opposite direction of rotation with 77.1429 mechanical degrees on the rotor circumference at each shift. By doing that, the generated wave represents a one-rotor tangential force density wave repetition cycle. The force density wave cycle is then decomposed by a 2D FFT decomposition tool to the rotor tangential force density harmonic spectrum. The error of the rotor tangential force density wave spectrum

TABLE 8. The simulation time and the maximum error observed for the three methods for calculating the rotor tangential force density wave components of the case study three-phase 6/4 SRM.

	Based on one mechanical cycle (4 electrical cycles)	Rotor tangential force repetition method (2/3 of an electrical cycle)	Fractional of an electrical cycle method (1/3 electrical cycle)
Time used FEA simulation for Force Calculation	12 p.u.	2 p.u.	1 p.u.
Maximum error in the displayed spectrum	0%	4%	4%

TABLE 9. The simulation time and the maximum error observed for the three methods for calculating the rotor tangential force density wave components of the case study three-phase 6/14 SRM.

	Based on one mechanical cycle (14 electrical cycles)	Rotor tangential force repetition method (7/3 of an electrical cycle)	Fractional of an electrical cycle method (1/3 electrical cycle)
Time used FEA simulation for Force Calculation	42 p.u.	7 p.u.	1 p.u.
Maximum error in the displayed spectrum	0%	0.45%	0.499%

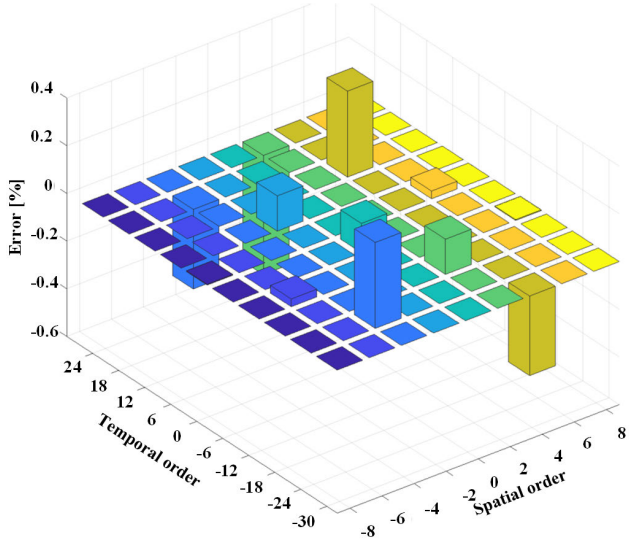

FIGURE 35. The error rotor tangential force density components obtained by the fractional of an electrical cycle method with respect to the components obtained by the one mechanical cycle method of the case-study 6/14 SRM.

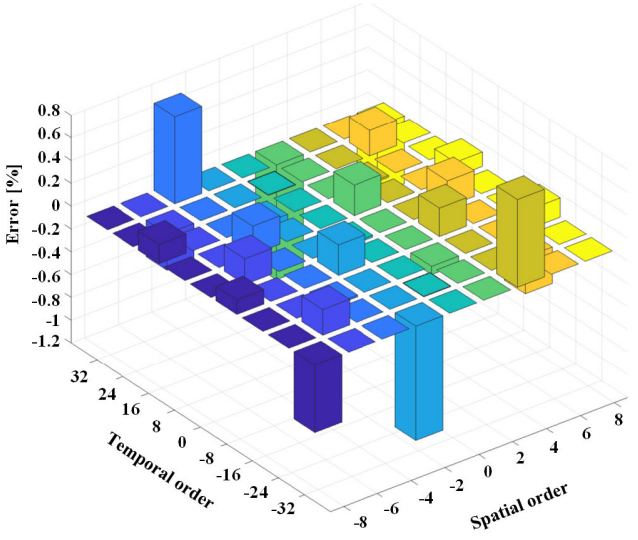

FIGURE 36. Rotor tangential force density components represented in the mechanical temporal order of a 8/6 SRM based on one radial force repetition generated (90 electrical degrees simulation).

obtained based on the fractional of an electrical cycle method is calculated with respect to the spectrum obtained based on the one mechanical cycle method (see Figure 35).

As shown in Figure 35, the maximum error observed for the method with respect to the one mechanical cycle method is about 0.49%. A comparison between the FE simulation time and the maximum error between the two proposed methods in this paper with respect to the one mechanical cycle method is summarized in Table 9.

The method is also used to generate the rotor tangential force density wave for the case study four-phase 8/6 SRM. As shown in Figure 16.b, the machine is needed to be simulated only for 1/4 of an electrical cycle. The rotor tangential force density wave results from the simulation of the machine for 1/4 of an electrical cycle is then shifted two times with 60 mechanical degrees on the rotor circumference opposite to the direction of rotor rotation at each shift. The generated wave from this process represents one rotor tangential force repetition. The rotor tangential force density wave is then decomposed with 2D FFT to the wave harmonics spectrum. The error is calculated for the rotor tangential force density harmonics obtained by the fractional of an electrical cycle method with respect to the tangential force density harmonics calculated based on the one mechanical cycle (see Figure 36). As indicated in Figure 36, the maximum error for the fractional of an electrical cycle method with respect to the one mechanical cycle method is about 1%. Table 9 summarizes the comparison of the three methods used for the calculation of tangential force density wave components.

As indicated from the case studies, the one rotor tangential force density wave repetition method significantly reduced the computational effort and time required for the rotor tangential force density wave spectrum calculation based on reducing the number of electrical cycles required. As indicated in this section, the amount of time reduction and the maximum error observed compared to the one mechanical cycle method depend on the machine's number of phases, stator teeth, and rotor teeth. The case studies also show the effectiveness of using the factional of an electrical cycle method for the generation of the rotor tangential force

TABLE 10. The simulation time and the maximum error observed for the three methods for calculating the rotor tangential force density wave components of the case study four-phase 8/6 SRM.

	Based on one mechanical cycle (6 electrical cycles)	Rotor tangential force repetition method (3/4 of an electrical cycle)	Fractional of an electrical cycle method (1/4 electrical cycle)
Time used FEA simulation for Force Calculation	24 p.u.	3 p.u.	1 p.u.
Maximum error in the displayed spectrum	0%	0.963%	1%

density waves. The method reduces the number of electrical cycles required for the rotor tangential force generation of any SRM configuration to $1/N_{ph}$, as indicated in section III and proved by the three case studies.

VI. CONCLUSION

This work presented a new fast method of generating the stator radial force density wave and the rotor tangential force density of switched reluctance motors. The method generates the full stator radial force density wave and the full rotor tangential force density wave by shifting the fractional electrical cycle radial force density wave data based on FE simulation of $1/N_{ph}$ of an electrical cycle. By simulating $1/N_{ph}$ of an electrical cycle, the stator radial force density wave and the rotor tangential force density wave can be estimated by using the proper shift angle and the proper circumferential number shifts of the regenerated parts, as illustrated in this paper. This results in a considerable computational cost reduction as compared to the existing method of using one electrical cycle or one mechanical cycle simulation. Three different SRMs configuration were simulated using different methods to demonstrate the effectiveness of the new method in reducing the required computational time for the radial and tangential force calculation. The proposed method also reduces the optimization time for geometry and topology optimizations of SRMs that target the mitigation of the stator radial force density, the torque ripples, and the rotor tangential force density.

ACKNOWLEDGMENT

The authors would like to thank Powersys Solutions for their support with JMAG software in this study.

REFERENCES

[1] M. Abdalmagid, E. Sayed, M. H. Bakr, and A. Emadi, "Geometry and topology optimization of switched reluctance machines: A review," *IEEE Access*, vol. 10, pp. 5141–5170, 2022.

[2] Y. Hu, C. Gan, W. Cao, J. Zhang, W. Li, and S. J. Finney, "Flexible fault-tolerant topology for switched reluctance motor drives," *IEEE Trans. Power Electron.*, vol. 31, no. 6, pp. 4654–4668, Jun. 2016.

[3] J. W. Jiang, B. Bilgin, and A. Emadi, "Three-phase 24/16 switched reluctance machine for a hybrid electric powertrain," *IEEE Trans. Transport. Electrific.*, vol. 3, no. 1, pp. 76–85, Mar. 2017.

[4] E. Bostanci, M. Moallem, A. Parsapour, and B. Fahimi, "Opportunities and challenges of switched reluctance motor drives for electric propulsion: A comparative study," *IEEE Trans. Transport. Electrific.*, vol. 3, no. 1, pp. 58–75, Mar. 2017.

[5] J. Lin, N. Schofield, and A. Emadi, "External-rotor 6–10 switched reluctance motor for an electric bicycle," *IEEE Trans. Transport. Electrific.*, vol. 1, no. 4, pp. 348–356, Dec. 2015.

[6] J. Liang, A. D. Callegaro, B. Howey, B. Bilgin, J. Dong, J. Lin, and A. Emadi, "Analytical calculation of temporal and circumferential orders of radial force density harmonics in external-rotor and internal-rotor switched reluctance machines," *IEEE Open J. Ind. Appl.*, vol. 2, pp. 70–81, 2021.

[7] E. Elhomdy, Z. Liu, and G. Li, "Thermal and mechanical analysis of a 72/48 switched reluctance motor for low-speed direct-drive mining applications," *Appl. Sci.*, vol. 9, no. 13, p. 2722, Jul. 2019.

[8] J. Liang, B. Howey, B. Bilgin, and A. Emadi, "Source of acoustic noise in a 12/16 external-rotor switched reluctance motor: Stator tangential vibration and rotor radial vibration," *IEEE Open J. Ind. Appl.*, vol. 1, pp. 63–73, 2020.

[9] J. Li, X. Song, and Y. Cho, "Comparison of 12/8 and 6/4 switched reluctance motor: Noise and vibration aspects," *IEEE Trans. Magn.*, vol. 44, no. 11, pp. 4131–4134, Nov. 2008.

[10] A. D. Callegaro, J. Liang, J. W. Jiang, B. Bilgin, and A. Emadi, "Radial force density analysis of switched reluctance machines: The source of acoustic noise," *IEEE Trans. Transport. Electrific.*, vol. 5, no. 1, pp. 93–106, Mar. 2019.

[11] M. Abdalmagid, M. Bakr, and A. Emadi, "A linesearch-based algorithm for topology and generative optimization of switched reluctance machines," *IEEE Trans. Transport. Electrific.*, early access, Feb. 15, 2023, doi: 10.1109/TTE.2023.3245992.

[12] B. Bilgin, J. W. Jiang, and A. Emadi, *Switched Reluctance Motor Drives: Fundamentals to Applications*. Boca Raton, FL, USA: CRC Press, 2018.

[13] S. Hosseini and Y. Alinejad-Beromi, "Noise reduction in switched reluctance motor by modifying the structures," *IET Electric Power Appl.*, vol. 14, no. 14, pp. 2863–2872, Dec. 2020.

[14] M. Belhadi, G. Krebs, C. Marchand, H. Hannoun, and X. Mininger, "Geometrical optimization of SRM on operating mode for automotive application," *Electr. Eng.*, vol. 100, no. 1, pp. 303–310, Mar. 2018.

[15] G. F. Lukman and J.-W. Ahn, "Radial force reduction method of switched reluctance motor with partial holes in the rotor," *J. Electr. Eng. Technol.*, vol. 17, no. 3, pp. 1775–1784, May 2022.

[16] M. E. Abdollahi, N. Vaks, and B. Bilgin, "A multi-objective optimization framework for the design of a high power-density switched reluctance motor," in *Proc. IEEE Transport. Electrific. Conf. Expo (ITEC)*, Jun. 2022, pp. 67–73.

[17] M. Zhang, I. Bahri, X. Mininger, C. Vlad, and E. Berthelot, "Vibration reduction control of switched reluctance machine," *IEEE Trans. Energy Convers.*, vol. 34, no. 3, pp. 1380–1390, Sep. 2019.

[18] P. Azer, B. Bilgin, and A. Emadi, "Mutually coupled switched reluctance motor: Fundamentals, control, modeling, state of the art review and future trends," *IEEE Access*, vol. 7, pp. 100099–100112, 2019.

[19] M. Elamin, "Acoustic noise mitigation of switched reluctance machines through skewing methods," M.S. thesis, Dept. Elect. Eng., Graduate Fac. Univ. Akron, OH, USA, 2017.

[20] M. Abdalmagid, M. Bakr, E. Sayed, and A. Emadi, "Adjoint sensitivity analysis of radial force components of switched reluctance machines," in *Proc. IEEE Transp. Electrific. Conf. Expo (ITEC)*, Chicago, IL, USA, Jun. 2021, pp. 395–400.

[21] A. D. Callegaro, B. Bilgin, and A. Emadi, "Radial force shaping for acoustic noise reduction in switched reluctance machines," *IEEE Trans. Power Electron.*, vol. 34, no. 10, pp. 9866–9878, Oct. 2019.

[22] J. Furqani, M. Kawa, K. Kiyota, and A. Chiba, "Comparison of current waveforms for noise reduction in switched reluctance motors," in *Proc. IEEE Energy Convers. Congr. Expo. (ECCE)*, Oct. 2017, pp. 752–759.

[23] J. Y. Chai, Y. W. Lin, and C. M. Liaw, "Comparative study of switching controls in vibration and acoustic noise reductions for switched reluctance motor," *IEE Proc.-Electric Power Appl.*, vol. 153, no. 3, p. 348, 2006.

[24] C. Ma, L. Qu, R. Mitra, P. Pramod, and R. Islam, "Vibration and torque ripple reduction of switched reluctance motors through current profile optimization," in *Proc. IEEE Appl. Power Electron. Conf. Exposit. (APEC)*, Mar. 2016, pp. 3279–3285.

[25] K. Diao, X. Sun, G. Lei, Y. Guo, and J. Zhu, "Multiobjective system level optimization method for switched reluctance motor drive systems using finite-element model," *IEEE Trans. Ind. Electron.*, vol. 67, no. 12, pp. 10055–10064, Dec. 2020.
[26] M. Omar, E. Sayed, M. Abdalmagid, B. Bilgin, M. H. Bakr, and A. Emadi, "Review of machine learning applications to the modeling and design optimization of switched reluctance motors," *IEEE Access*, vol. 10, pp. 130444–130468, 2022.
[27] S. Li, S. Zhang, T. G. Habetler, and R. G. Harley, "Modeling, design optimization, and applications of switched reluctance machines—A review," *IEEE Trans. Ind. Appl.*, vol. 55, no. 3, pp. 2660–2681, May 2019.
[28] J. Liang, A. D. Callegaro, B. Bilgin, and A. Emadi, "A novel three-dimensional analytical approach for acoustic noise modeling in switched reluctance machines," *IEEE Trans. Energy Convers.*, vol. 36, no. 3, pp. 2099–2109, Sep. 2021.

MOHAMED ABDALMAGID (Graduate Student Member, IEEE) received the B.Sc. degree (Hons.) in electrical engineering from the Shoubra Faculty of Engineering, Benha University, Cairo, Egypt, in 2011, and the M.Sc. degree in electrical engineering from the Faculty of Engineering, Cairo University, Giza, Egypt, in 2017. He is currently pursuing the Ph.D. degree in electrical engineering with the McMaster Automotive/Aerospace Resource Centre, McMaster University, Hamilton, ON, Canada. He was a Research Assistant with the Electronics Research Institute, Cairo, from 2013 to 2018. He is involved in many industrial projects, where he designs and tests various configurations of axial flux permanent magnet motor for aerospace propulsion application. His research interests include axial flux permanent magnet (PM) motor design, switched reluctance motor (SRM) design, and the optimization of SRM design for automotive/aerospace applications.

MOHAMED H. BAKR (Senior Member, IEEE) received the B.Sc. degree (Hons.) in electronics and communications engineering and the master's degree in engineering mathematics from Cairo University, Egypt, in 1992 and June 1996, respectively, and the Ph.D. degree from the Department of Electrical and Computer Engineering, McMaster University, in September 2000. In November 2000, he joined the Computational Electromagnetics Research Laboratory (CERL), University of Victoria, Victoria, Canada, as an NSERC Postdoctoral Fellow. His research interests include optimization methods, computational electromagnetics, computer-aided design, the modeling of power circuits and motors, microwave circuits, THz, and photonic devices, nanotechnology, artificial intelligence and its applications, the smart analysis of high frequency structures, and efficient optimization using time/frequency domain methods. He received the Premier's Research Excellence Award (PREA) from the province of Ontario, Canada, in 2003. He also received an NSERC Discovery Accelerator Supplement (DAS) Award, in 2011. In 2014, he was a co-recipient of the Chrysler's Innovation Award for project on novel designs of hybrid cars. He was awarded a Leadership in Teaching and Learning (LTL) Fellowship from the McPherson Institute, McMaster University, in April 2018. In 2020, he was a recipient of the Faculty Appreciation Award by the McMaster Engineering Society (MES). In April 2021, he was awarded the President's Award for Outstanding Contributions for Teaching and Learning from McMaster University. In July 2021, he was awarded a Distinguished Engineering Educator honorific from the Faculty of Engineering, McMaster University. He was also included in Stanford's list of the top 2% most cited scientists for the years (2020–2022). He was selected as the Chair of the Department of Electrical and Computer Engineering, McMaster University, for five years starting July 2022.

ALI EMADI (Fellow, IEEE) received the B.S. and M.S. degrees (Hons.) in electrical engineering from the Sharif University of Technology, Tehran, Iran, in 1995 and 1997, respectively, and the Ph.D. degree in electrical engineering from Texas A&M University, College Station, TX, USA, in 2000. He is currently the Canada Excellence Research Chair Laureate of McMaster University, Hamilton, ON, Canada. He is also the holder of the NSERC/FCA Industrial Research Chair of Electrified Powertrains and the Tier I Canada Research Chair of Transportation Electrification and Smart Mobility. Before joining McMaster University, he was the Harris Perlstein Endowed Chair Professor of Engineering and the Director of the Electric Power and Power Electronics Center and Grainger Laboratories, Illinois Institute of Technology, Chicago, where he established research and teaching facilities and courses in power electronics, motor drives, and vehicular power systems. He was the Founder, the Chairperson, and the President of Hybrid Electric Vehicle Technologies Inc., (HEVT)—a university spin-off company of Illinois Tech. He is also the President and the Chief Executive Officer of Enedym Inc., and Menlolab Inc.,-two McMaster University spin-off companies. He is the principal author/coauthor of over 700 journals and conference papers and several books, including *Vehicular Electric Power Systems*, in 2003, *Energy Efficient Electric Motors*, in 2004, *Uninterruptible Power Supplies and Active Filters*, in 2004, *Modern Electric, Hybrid Electric, and Fuel Cell Vehicles* (Second Edition, 2009), and *Integrated Power Electronic Converters and Digital Control*, in 2009. He is also an Editor of the *Handbook of Automotive Power Electronics and Motor Drives*, in 2005, and *Advanced Electric Drive Vehicles*, in 2014. He was the Co-Editor of the *Switched Reluctance Motor Drives: Fundamentals to Applications*, in 2018. He was the Inaugural General Chair of the 2012 IEEE Transportation Electrification Conference and Expo (ITEC) and has chaired several IEEE and SAE conferences in the areas of vehicle power and propulsion. He was the founding Editor-in-Chief of the IEEE TRANSACTIONS ON TRANSPORTATION ELECTRIFICATION, from 2014 to 2020.